Journal of Materials Chemistry C

Accepted Manuscript

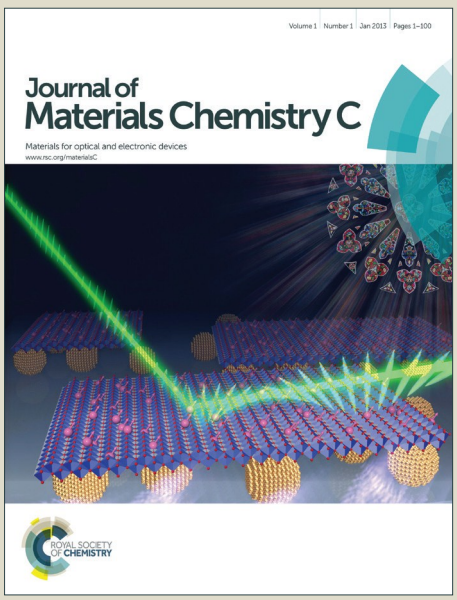

ROYAL SOCIETY OF CHEMISTRY

www.rsc.org/materialsC

Journal Name

ARTICLE

A Thermally Stable and Reversible Microporous Hydrogen-Bonded Organic Framework: Aggregation Induced Emission and Metal Ion-sensing Properties†

Received 00th January 20xx,
Accepted 00th January 20xx

DOI: 10.1039/x0xx00000x

www.rsc.org/

Hui Zhou,[a] Qun Ye,[a] Xiangyang Wu,[b] Jing Song,[a] Ching Mui Cho,[a] Yun Zong,[a] Ben Zhong Tang,*[c] T. S. Andy Hor,[a,d] Edwin Kok Lee Yeow,[b] and Jianwei Xu*[a,d]

A microporous hydrogen-bonded organic framework (HOF) derived from a polyhedral oligomeric silsesquioxane (POSS) intermediate and an aggregation-induced emission (AIE) luminogen tetraphenylethene (TPE) derivative has been synthesized and structurally characterized by various methods. This unique HOF exhibits a permanent porosity with the Brunauer-Emmett-Teller (BET) surface area of 101.9 m^2/g. This HOF could be well dispersed in organic solvents in a form of nanoparticles with a size of a few hundred nanometers. These nanoparticles are highly fluorescent in organic solution, and exhibit a high fluorescence quenching selectivity towards copper ion. Furthermore, the fluorescence of this HOF could be recovered by removal of copper ion upon addition of cyanide and, more interestingly, this process could be repeated several times without considerably sacrificing the sensing activity towards copper ion.

Introduction

Recently, porous hydrogen bonded organic frameworks (HOFs) have attracted increasing interest as stimuli sensitive materials,[1] but HOFs have lagged significantly behind metal-organic frameworks in terms of framework design, topological rationalization and functionalization. This is because hydrogen bonds are weaker and more flexible in conformation when compared to coordination interactions in other frameworks, such as zeolites and metal-organic frameworks (MOFs),[2] leading to lower stabilities.[3,4] Thousands of HOFs have been prepared during the last decades, but HOFs with permanent porosity are rarely offered, as HOFs easily collapse once the guest molecules are removed from the super-molecular network system. To the best of our knowledge, only very limited HOFs display high thermal stability and exhibit permanent porosity after removal of guest molecules, in which the host molecules can form strong hydrogen bonds and π-π stacking each other.[5] Therefore, it is still challenging to obtain porous HOFs, which are stable enough for their potential applications as storage and separation, heterogeneous catalysis, sensing and so on.

Aggregation-caused quenching (ACQ) of fluorescence is commonly observed in fluorescent materials in solid state, which has undermined its potential for solid-state sensors or probes.[6] Recently, AIE materials have attracted increasing interest in the areas of optoelectronics and sensory systems due to the absence of ACQ effect.[7] However, the stimuli sensitive HOFs materials with AIE properties have been rarely reported, and their sensing application was not found mainly due to the lack of suitable processable HOFs materials with AIE activity, which is tolerant to solvents, moisture, temperature, etc.[8]

Herein, we report on a feasible method without using any guest molecules to prepare AIE active HOF, which responds to the external stimuli. This HOF (POSS-T_8A) was prepared by the condensation of AIE precursor 4-(1,2,2-triphenylvinyl)benzoic acid and octa(amino)-substituted POSS derivative (Scheme 1). For comparison, another analogue POSS-T_8B with ester linkages was prepared as well. POSS have been demonstrated as effective building blocks to generate porous materials through thermolysis,[9] hydrosylation,[10] coupling reactions,[11] as well as free radical copolymerization with other monomers.[12] Several porous materials derived from octa(vinyl)-POSS exhibit BET surface area as high as 700 m^2/g and maximum tunable mesopore volume of 2.0 cm^3/g.[13] In this paper, POSS-T_8A molecules show enhanced AIE properties,

[a]Institute of Materials Research and Engineering, Agency for Science, Technology and Research (A*STAR), 3 Research Link, Singapore 117602. E-mail: jw-xu@imre.a-star.edu.sg
[b]Division of Chemistry and Biological Chemistry, School of Physical and Mathematical Sciences, Nanyang Technological University, 21 Nanyang Link, Singapore 637371.
[c]Department of Chemistry, The Hong Kong University of Science & Technology, Clear Water Bay, Kowloon, Hong Kong, China. E-mail: tangbenz@ust.hk
[d]Department of Chemistry, National University of Singapore, 3 Science Drive 3, Singapore 117543.
† Electronic supplementary information (ESI) available: Experimental details, NMR spectra, FTIR spectra and MALDI-TOF spectra. See DOI: xxxxxxxxxx

and display high sensitivity (Stern-Volmer co-efficient K_{sv} = 30305 M^{-1}) and fluorescence quenching selectivity for Cu^{2+} ion due to the presence of amide linkages, which is effectively able to bind with Cu^{2+} ion, leading to the conformation change of TPE units in the POSS-T_8A molecules and eventually resulting in fluorescence turn-off (Scheme 1). This is the first demonstration for the fluorescence signaling *via* conformational changes of pendent luminogen moieties in HOFs materials.

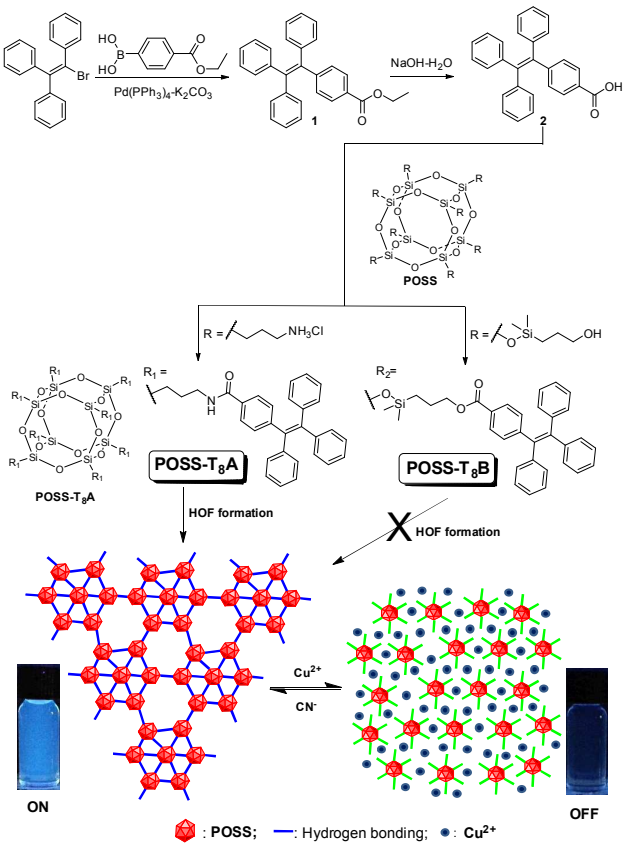

Scheme 1 Synthetic route leading to POSS-T_8A, POSS-T_8B, and structural illustration of POSS-T_8A for Cu^{2+} sensing.

Results and Discussion

POSS-T_8A and POSS-T_8B were prepared using a similar method as shown in Scheme 1. POSS-T_8B was easily purified by column chromatography. In contrast, POSS-T_8A was first purified by precipitating diluted POSS-T_8A $CHCl_3$ solution in methanol. Then resulting material was isolated by centrifugation, and then collected solid residue was washed with hexane and methanol followed by Soxhlet extraction with Et_2O. Both POSS-T_8A and POSS-T_8B were well characterized by ^{1}H, ^{13}C and ^{29}Si nuclear magnetic resonance (NMR), matrix-assisted laser desorption ionization time of flight (MALDI TOF) mass spectrometer and elemental analysis. POSS-T_8B shows very good solubility in most organic solvents such as chloroform, tetrahydrofuran (THF), ethyl acetate (EA); however, POSS-T_8A is only fully soluble in pyridine but well-dispersed in other common organic solvents such as THF, chloroform, EA, etc., in a form of nanoparticles. This indicates that POSS-T_8A molecules form hydrogen-bonded aggregates, which limits the solubility in organic solvents. Good solubility in pyridine is due to the fact that pyridine can act as electron acceptors to form hydrogen bonds with amide linkages and hence dissociate the self-aggregation of the POSS-T_8A molecules. This is confirmed by the ^{1}H NMR study of POSS-T_8A in pyridine-d_5 and DMSO-d_6. The proton signals of POSS-T_8A in pyridine-d_5 are readily identified, while its protons in DMSO-d_6 were not observed under the same condition (Fig. S10). In contrast, the ester linkages do not facilitate to form any strong hydrogen-bonded networks and no hydrogen-bonded self-aggregation was observed for POSS-T_8B molecules. Therefore, POSS-T_8B shows very good solubility in many organic solvents. The nanoparticle structure of POSS-T_8A was characterized by dynamic light scattering and it forms nanoparticles with an average size of 291.4 nm in DMSO, which was supported by transmission electron microscope (TEM) analysis (Fig. 1a and 1b). Both POSS-T_8A and POSS-T_8B (Fig. 1c and S1) exhibited good thermal stability in air with a decomposition temperature of more than 370 °C.

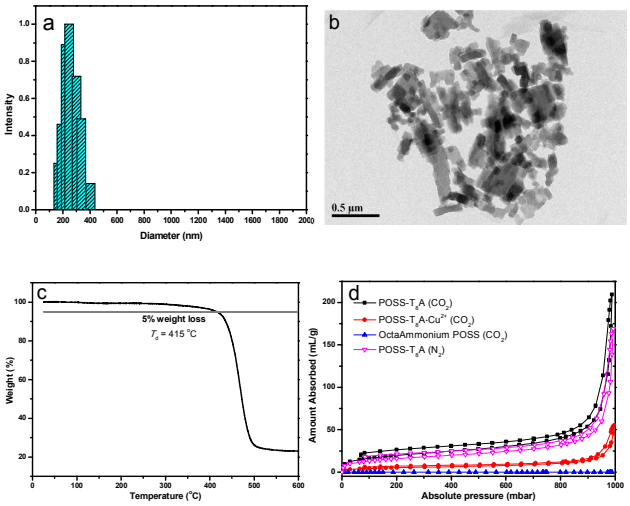

Fig. 1 (a) Particle size distribution of POSS-T_8A in DMSO. (b) TEM image of POSS-T_8A particles prepared in the DMSO; scale bar is 0.5 μm. (c) TGA thermogram of POSS-T_8A recorded at a heating rate of 20 °C/min in air. (d) Gas absorption isotherms for POSS-T_8A, POSS-T_8A•Cu^{2+} and Octa(NH_2)-POSS (CO_2 at 0 °C, N_2 at -196 °C).

Physical gas adsorption is widely used to study the pore characteristics of solid materials.[14] The porosity of POSS-T_8A was studied by CO_2 gas adsorption and desorption at 273 K (Fig. 1d). POSS-T_8A shows type II isotherms with a significant amount of CO_2 adsorbed at low pressure (P/P_0 < 0.03), followed by a much increased adsorption at higher pressure (P/P_0 > 0.9) attributable to gas condensation into voids among particles. The CO_2 adsorption capacity was measured by CO_2 isothermal adsorption at 273 K. The micropore BET surface area is calculated to be 101.9 m^2/g in terms of Dubinin–Astakhov method. The pore size distribution was evaluated by applying a non-local density functional theory (NLDFT) model. The NLDFT model was applied under the assumption that the slit-shaped pores have uniformly dense carbon walls and that

the adsorbate is a fluid of hard spheres. Additionally, the interaction between adsorbent and adsorbate was considered on their elemental species by a soft program installed on the BET apparatus. The pore width was distributed mainly in the micropore range, especially in the range of 0.5-0.9 nm (Fig. S2).

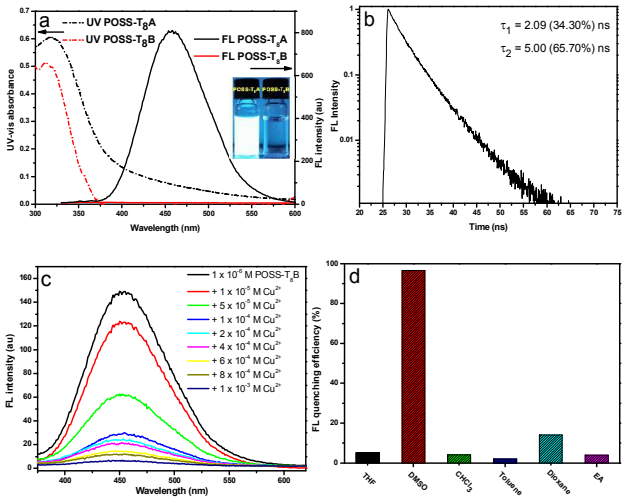

Fig. 2 (a) UV-Vis and fluorescence spectra of POSS-T_8A and POSS-T_8B in THF. Insert is the photographs of samples under UV in THF taken under UV illumination (λ_{ex} = 365 nm), [C] = 1.0 × 10^{-5} M. (b) The time-resolved fluorescence lifetimes of POSS-T_8A in THF under excitation of a femtosecond pulsed laser at 375 nm. (c) Fluorescence titration spectra of POSS-T_8A upon addition of $Cu(NO_3)_2$ in DMSO. λ_{ex} = 314 nm, [POSS-T_8A] = 1.0 × 10^{-6} M. (d) Fluorescence quenching efficiency of POSS-T_8A with Cu^{2+} ion in various solvents, [POSS-T_8A] = 1.0 × 10^{-6} M, [Cu^{2+}] = 1.0 × 10^{-3} M.

POSS-T_8A shows strong blue-white emission both in solid state and organic solvents (Fig. 2). POSS-T_8A could be dispersed in organic solvents, such as THF, chloroform and DMSO, to form macroscopically homogeneous but visually transparent solutions without observing any precipitates. Taking the mixture of POSS-T_8A in THF as an example, no tendency towards agglomeration was observed when the dispersion was stored at 4 ^{o}C for 6 months. Typically, most of TPE-containing materials are non-emissive in good solvents, such as THF. However, as shown in Fig. 2a, dispersion of POSS-T_8A displays strong fluorescent emission with an emission maximum at 458 nm and a wide of spectrum ranging from 375 nm to 600 nm, which can be seen even by naked eyes under the bright light when UV illuminated when the concentration is as low as 1.0 × 10^{-5} M. On the contrary, POSS-T_8A is not fluorescent in pyridine as it is completely soluble in it without forming any nanoparticles like in other organic solvents (Fig. S3). Similarly, POSS-T_8B displays normal AIE properties, as shown in Fig. S4, and its fluorescence would be turned on in the mixture of THF/H_2O, when the water volume fraction is increased up to 60%. Considering enhanced AIE property and morphology of POSS-T_8A particles, together with the amides' nature to form hydrogen bonds, it is therefore confirmed that the amide groups of POSS-T_8A form the hydrogen-bonded networks (Scheme 1). Within this HOFs structure, the restricted intra- and inter-molecular rotation blocks the non-radiative channel and further enhances the light emission. The time-resolved fluorescence spectrum of POSS-T_8A was examined and it exhibited dual exponential decay with a life-time of 2.09 and 5.00 ns (Fig. 2b).

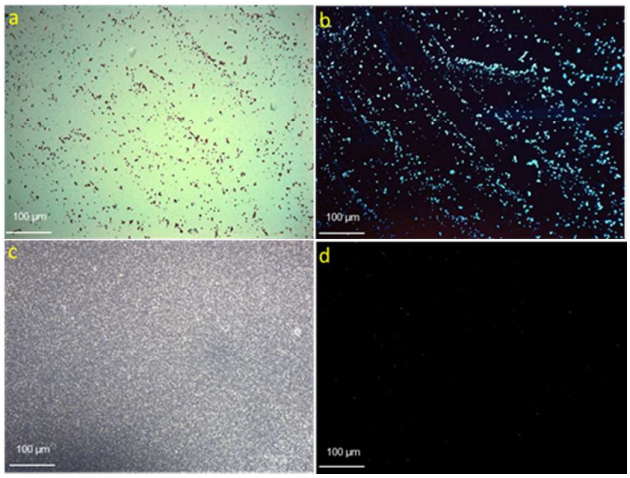

Fig. 3 Enlarged image (a) and fluorescent image (b) of POSS-T_8A nanoparticles. Enlarged image (c) and fluorescent image (d) of POSS-T_8A•Cu^{2+} nanoparticles. Photography is taken under a fluorescence microscope with a 337 nm excitation. Scale bar is 100.0 μm.

The fluorescence titration of POSS-T_8A with Cu^{2+} in DMSO showed a progressive decrease in fluorescence intensity of POSS-T_8A upon addition of Cu^{2+} ion (Fig. 2c). It was known that Cu^{2+} ion is able to coordinate with nitrogen atoms of the amide groups[15] and quench the fluorescence.[16] In our case, Cu^{2+} ion can quench the fluorescence in different organic solvents and it shows the highest quenching efficiency in DMSO (Fig. 2d). The fluorescence microscopy also clearly showed that the fluorescent nanoparticles appeared non-fluorescent upon addition of enough Cu^{2+} ion (Fig. 3b and 3d).

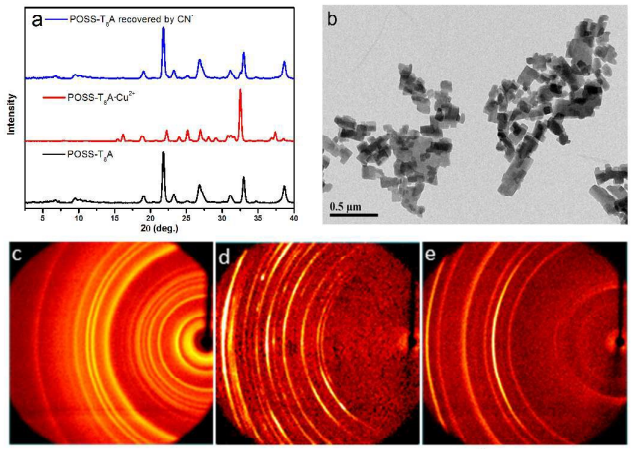

Fig. 4 (a) PXRD pattern of POSS-T_8A, POSS-T_8A•Cu^{2+} and POSS-T_8A recovered by CN^-. (b) TEM image of POSS-T_8A particles recovered by CN^-. Electron diffraction (ED) patterns of POSS-T_8A (c), POSS-T_8A•Cu^{2+} (d), and POSS-T_8A recovered by CN^- (e).

Wide angle X-ray diffractograms of POSS-T_8A and POSS-T_8A•Cu^{2+} are illustrated in Fig. 4a. A very weak broad scattering at 9.48° corresponding to *d*-spacing of 9.33 Å is observed for POSS-T_8A, which is due to the Si-O clusters in the POSS core.[17] The POSS-T_8A is crystalline as evidenced by a group of the sharp reflection peaks from 2ϑ = 19.04° (4.66 Å, 2nd order diffraction, 200), to 38.66° (2.33 Å). Upon addition of Cu^{2+} ion, the diffraction profile of POSS-T_8A•Cu^{2+} completely differs from the POSS-T_8A; however recovered POSS-T_8A goes back to the same diffraction pattern as the pristine POSS-T_8A after Cu^{2+} ion is removed by CN^{-1}, which is also supported by the similar TEM image (Fig. 4b), revealing the excellent reversibility of this HOF structure.

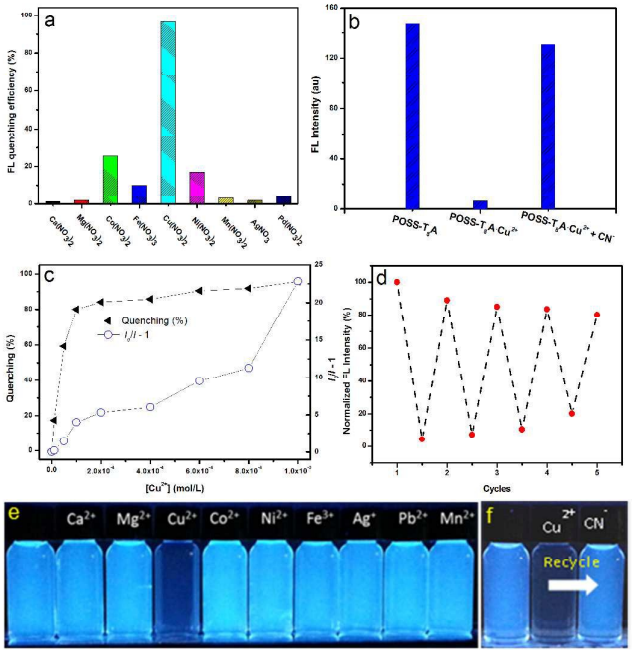

Fig. 5 (a) Fluorescence quenching efficiency of POSS-T_8A upon addition of various metal ions. λ_{ex} = 314 nm. (b) Fluorescence intensity changes during sensing and recovering by CN^-. (c) Concentration-dependent fluorescence quenching of POSS-T_8A by Cu^{2+}. (d) The fluorescence recovery of POSS-T_8A on addition of CN^-. (e) Photographs of samples with and without addition of metal ions under UV illumination (365 nm). [POSS-T_8A] = 1.0 × 10^{-6} M, [ion] = 1.0 × 10^{-3} M. (f) Photographs of POSS-T_8A, POSS-T_8A•Cu^{2+} and POSS-T_8A•Cu^{2+} with tetrabutylammonium cyanide under UV illumination (365 nm). [POSS-T_8A] = 1.0 × 10^{-6} M, [Cu^{2+}] = 1.0 × 10^{-3} M, [CN^-] = 1.0 × 10^{-2} M.

The fluorescence response of POSS-T_8A to other metal ions was also studied. As shown in Fig. 5a, transition metal ions, such as Mn^{2+}, Co^{2+}, Ni^{2+}, and Fe^{3+} exhibited limited fluorescence quenching with 10 - 26% efficiency. In contrast, almost no fluorescence quenching was observed for alkaline-earth metal ions, such as Mg^{2+} and Ca^{2+} ions. In contrast, the Cu^{2+} ion shows the highest quenching efficiency (97%). Specifically, the quenching effect of metal ions was quantified by the Stern-Volmer equation (Table 1).[16] The largest quenching coefficient (K_{sv}) value was obtained for Cu^{2+} ion to be 30305 M^{-1} (Fig. 5c), which is much higher than 7847 M^{-1} of MOFs material CPP-16.[18] The selective response to metal ions was visualized in Fig. 5e. The influence of interrupting Cu^{2+} ion sensing by other metal ions was studied by conducting Cu^{2+} sensing in the presence of many other metal ions. Emission spectra (Fig. S5) described no disturbance on selective Cu^{2+} sensing by any of the other metal ions. It is worthy to note that the quenched fluorescence could be recovered by addition of tetrabutylammonium cyanide (Fig. 5b and 5f), and the recovered HOFs material still displayed sensing ability to Cu^{2+} ion. After 4 off-on cycles (Fig. 5d), the fluorescence quenching towards to Cu^{2+} ion still remained around 80%, suggesting high reversibility and responsiveness of POSS-T_8A based HOFs structure.

Table 1 Fluorescence Quenching Coefficients (K_{sv}) of POSS-T_8A on Different metal Ions

Metal ions	K_{sv} [M^{-1}]	Metal ions	K_{sv} [M^{-1}]
Ca^{2+}	11	Fe^{3+}	111
Mg^{2+}	20	Ag^{+}	17
Cu^{2+}	30305	Pd^{2+}	43
Co^{2+}	346	Mn^{2+}	33
Ni^{2+}	206		

Conclusions

In conclusion, we reported on two AIE-active POSS based molecules. POSS-T_8B with ester linkages did not form HOF and only showed a normal AIE property. Being different from usual HOF materials,[1,5] POSS-T_8A with amide linkages enables to form very stable super-molecular HOF structure without the assistance of any guest molecules. This HOF showed enhanced AIE activity in solutions. Specific response of POSS-T_8A to Cu^{2+} ion led to the dissociation of HOFs structure and subsequent release of the restricted intramolecular rotation of TPE moieties so as to activate their non-radiative channel and as a result turn off the emission. The fluorescence of POSS-T_8A and HOF structure could be recovered by removal of Cu^{2+} ion by addition of CN^- ion to form more stable $Cu(CN)_x^{2-x}$ species.[18] This type of AIE-active POSS-based HOF materials could be used as a promising chemosensor for potential applications in the detection of Cu^{2+} ion as well as for gas storage and separation provided POSS structures are appropriately tailored with desired substituents.

Experimental

General.

All synthetic manipulations were carried out under an atmosphere of dry argon gas using standard vacuum-line Schlenk techniques. 1-Bromotriphenylethylene was purchased from Tokyo Chemical Industry Co., Ltd. All solvents were degassed and purified before use according to standard literature methods. Diethyl ether, hexanes, tetrahydrofuran, and toluene were purchased from Aldrich Chemical Co. Inc. and distilled from sodium/benzophenone ketyl before use. Other commercially available reagents and solvents were used as received.

Instrumentation.

^{1}H and ^{13}C nuclear magnetic resonance (NMR) spectra were recorded on a Bruker DRX 400-MHz NMR spectrometer in $CDCl_3$ at room temperature using tetramethylsilane (TMS) as an internal standard. Operating frequencies of the NMR spectrometer were 400.13 MHz (^{1}H), 100.61 MHz (^{13}C) and 79.49 MHz (^{29}Si). Electron impact mass spectra (EIMS) and high resolution MS (HRMS) were recorded using a Micromass 7034E mass spectrometer. Elemental analysis was conducted on a Perkin-Elmer 240C elemental analyzer for C, H, and N determination. UV-vis and fluorescence spectra were obtained using a Shimadzu UV3101PC UV-vis-NIR spectrophotometer and a Perkin-Elmer LS 50B luminescence spectrometer with a Xenon lamp as light source, respectively. Thermal analysis was performed on a Perkin-Elmer thermogravimetric analyzer (TGA 7) in nitrogen or in air at a heating rate of 20 °C/min and on a TA Instruments Differential Scanning Calorimetry (DSC) 2920 at a heating rate and a cooling rate of 5 °C min^{-1} in nitrogen. Dynamic light scattering experiments were performed on a Brookhaven 90 plus spectrometer with a temperature controller. An argon ion laser operating at 633 nm was used as light source. ASAP 2020 surface area analyzer was used to measure gas adsorption isotherms. To have a guest-free framework, the sample was purified by successive Soxhlet extraction with methanol, ethyl acetate, 1,4-dioxane and chloroform. The result product was vacuumed at room temperature for 24 hours followed by 100 °C until the outgas rate was 5 mmHg/min prior to measurements. A sample of 187.9 mg was used for the sorption measurement and was maintained at 77 K with liquid nitrogen, at 273 K with an ice–water bath. The CO_2 adsorption capacity was measured by CO_2 isothermal adsorption at 273 K. Furthermore, the parameters of the Dubinin–Astakhov equation:

$$\log(V) = \log(V_0) - \left[\frac{RT}{\beta E_0}\right]^n \left[\log\left(\frac{P_0}{P}\right)\right]^n$$

were obtained from CO_2 adsorption. P, P_0, V, V_0, n, R, E_0, and β are the equilibrium pressure, the saturation vapor pressure of the gas at the analysis temperature (T), the volume adsorbed at equilibrium pressure, the monolayer capacity, the Astakhov exponent, the gas constant, characteristic energy, and the affinity coefficient of the analysis gas, respectively.

Synthesis of compounds.

Generally procedures. As shown in Scheme 1, POSS-T_8A was synthesized from a 4-(1,2,2-triphenylvinyl)benzoic acid (**2**), which was synthesized by two steps with 91% yield staring from 1-bromotriphenylethylene. After that, compound **2** reacts with octa-ammonium POSS in the present of 1-hydroxybenzotriazole and *N*,*N*′-dicyclohexylcarbodiimide to generate POSS-T_8A with reasonable yield of 70%. POSS-T_8A was structurally characterized by various spectroscopic methods and elemental analysis. The ^{1}H NMR spectrum of POSS-T_8A is illustrated in Fig. S6. The presence of signals at δ 7.54 and 7.09-6.90 with an integration ratio of 2 : 17, which were assigned to protons of tetraphenylethene (TPE). Furthermore, the integration ratio for signals at δ 7.54, 3.11, 1.51 and 0.58 is 1 : 1 : 1 : 1. Those ^{1}H NMR data together with results of MALDI-TOF indicate that eight TPE moieties are introduced into octa-ammonium POSS successfully. Similarly, POSS-T_8B can be prepared through the same route by 3 steps with overall yield as 53%. All of those POSS materials are structurally characterized by various spectroscopic methods and elemental analysis.

Ethyl 4-(1,2,2-triphenylvinyl)benzoate (**1**). Bromotriphenylethylene (670.5 mg, 2.00 mmol), 4-(ethoxycarbonyl)phenylboronic acid (456.2 mg, 2.40 mmol), Na_2CO_3 (2.76 g, 20.00 mol) and $Pd(PPh_3)_4$ (115.6 mg, 0.10 mmol) were placed in a Schlenk flask and the flask was evacuated and recharged with Ar gas. Toluene (40.0 mL), ethanol (10.0 mL) and water (10.0 mL) was added, then the resulting mixture was degassed for 30 min and the mixture was stirred for 12 h at 110 °C under Ar gas. After cooling to room temperature, the mixture was poured into saturated aqueous $NaHCO_3$, extracted with dichloromethane (3 × 40.0 mL), dried over Na_2SO_4, filtered, and evaporated. The resulting residue was purified by chromatography over silica gel eluting with

hexane-dichloromethane (1 : 4), affording compound as an off white solid 862.2 mg (92.0%). ^{1}H NMR ($CDCl_3$): δ 7.77 (d, 2H, J = 8.6 Hz), 7.10 (m, 11H), 7.01 (m, 6H), 4.32 (q, 2H, J = 7.1 Hz), 1.35 (t, 3H, J = 7.3 Hz). ^{13}C NMR ($CDCl_3$): δ 166.7, 148.9, 143.4, 143.3, 142.6, 142.5, 140.1, 131.5, 131.4, 129.1, 128.0, 127.8, 127.0, 126.9, 126.8, 60.9, 14.4. IR (thin film): ν = 3420, 3052, 3020, 2979, 1950, 1810, 1714, 1603, 1492, 1443, 1274, 1176, 1102, 1020, 762, 749, 699 cm^{-1}. HRMS (ESI): [M + H$^+$] calcd for $C_{29}H_{25}O_2$, m/z 405.1855; found, m/z 405.1855.

4-(1,2,2-triphenylvinyl)benzoic acid (**2**). To the solution of methyl 4-(1,2,2-triphenylvinyl)benzoate (**1**) (808.4 mg, 2.00 mmol) in mixture of THF (10 mL) and H_2O (10 mL) was added NaOH (240 mg, 6 mmol). The resulting solution was stirred for 12 h at 90 ^{o}C under Ar gas. After cooling to room temperature, pH value of the mixture was adjusted to 4.0 by 1 M HCl solution, then extracted with dichloromethane (3 × 40.0 mL), dried over Na_2SO_4, filtered, and evaporated. The resulting residue was purified by chromatography over silica gel eluting with Ethyl acetate-dichloromethane (1 : 10), affording compound **2** as an off white solid 744.7 mg (99.0%). ^{1}H NMR ($CDCl_3$): δ 7.80 (d, 2H, J = 8.3 Hz), 7.11 (m, 11H), 7.02 (m, 6H). ^{13}C NMR ($CDCl_3$): δ 171.4, 149.9, 143.3, 143.2, 143.1, 142.8, 140.0, 131.6, 131.4, 129.8, 128.0, 127.9, 127.1, 127.0, 126.9. IR (thin film): ν = 3422, 3049, 2947, 1720, 1604, 1491, 1443, 1404, 1368, 1283, 1177, 1104, 1075, 1020, 749, 700 cm^{-1}.HRMS (ESI): [M - H$^+$] calcd for $C_{27}H_{19}O_2$, m/z 375.1391; found, m/z 375.1385.

POSS-T_8A. 1-Hydroxybenzotriazole (HOBT, 67.5 mg, 0.50 mmol), 4-(1,2,2-triphenylvinyl)benzoic acid (188.0 mg, 0.50 mmol), and OctaAmmonium POSS (58.7 mg, 0.05 mmol) are dissolved in dry DMF (2.0 mL). After addition of triethylamine (69.5 µL, 0.50 mmol), the stirred solution is cooled in an ice-water bath and *N*,*N*′-dicyclohexylcarbodiimide (103.0 mg, 0.50 mmol) is added. The resulting mixture is stirred at room temperature for 5 days, then ethyl acetate (50.0 mL) is added and the mixture is washed with Mill-Q water (4 × 100.0 mL). After dried of the collected organic phase, the crude product was first purified by precipitating POSS-T_8A's diluted solution in a large amount of $CHCl_3$ by methanol. Then resulting material was isolated by centrifugation, and then collected solid residue was washed with hexane and methanol followed by Soxhlet extraction with Et_2O, affording product POSS-T_8A as a white powder (142.4 mg, 77%). ^{1}H NMR (400.13 MHz, DMSO-d_6): δ 8.33 (m, 1H), 7.54 (d, 2H, J = 8.4 Hz), 7.09-6.90 (m, 17H), 3.11 (m, 2H), 1.51 (m, 2H), 0.58 (m, 2H). ^{1}H NMR (400.13 MHz, pyridine-d_5): δ 9.10 (m, 1H), 8.12 (d, 2H, J = 8.8 Hz), 7.28 (d, 2H, J = 8.47 Hz), 7.21-7.15 (m, 15H), 3.68 (m, 2H), 1.99 (m, 2H), 0.93 (m, 2H). ^{13}C NMR (100.61 MHz, pyridine-d_5): δ 168.0, 147.6, 144.4, 144.3, 144.2, 142.8, 141.2, 134.4, 132.2, 132.1, 128.8, 128.7, 128.0, 127.7, 127.6, 127.5, 43.3, 24.0, 10.1. ^{29}Si NMR (79.49 MHz, pyridine-d_5): δ -59.2. IR (thin film): ν = 3432, 3340, 3054, 2930, 2868, 1639, 1607, 1538, 1493, 1444, 1303, 1195, 1111, 1030, 861, 760, 749, 698, 628 cm^{-1}. MALDI-TOF: [M + H$^+$] calcd for $C_{240}H_{209}N_8O_{20}Si_8$, m/z 3750.03; found, m/z 3750.20. Anal. Calcd for $C_{240}H_{208}N_8O_{20}Si_8$: C, 76.89; H, 5.59; N, 2.99; Si, 5.99. Found: C, 76.81; H, 5.71; N, 2.95; Si, 5.93.

POSS-T_8B. 1-Hydroxybenzotriazole (HOBT, 67.5 mg, 0.50 mmol), 4-(1,2,2-triphenylvinyl)benzoic acid (188.0 mg, 0.50 mmol) and Pss-octa[C3-hydoxypropyl)dimethyl-siloxy]subsitituted (74.3 mg, 0.05 mmol) are dissolved in dry DMF (2.0 mL). After the stirred solution is cooled in an ice-water bath, *N*,*N*′-dicyclohexylcarbodiimide (103.0 mg, 0.50 mmol) is added. After stirring at room temperature for 5 days, ethyl acetate (50.0 mL) is added and the mixture is filtered. The solution is washed with saturated NaCl solution (2 × 100.0 mL). The organic solution is dried over anhydrous $MgSO_4$, then the solvent is removed *in vacuo* and resulting crude product is purified by flash chromatography with ethyl acetate-hexane (1:4), affording product POSS-T_8B as a light yellow semi solid (126.0 mg, 58%). ^{1}H NMR (400.13 MHz, $CDCl_3$): δ 7.77 (d, 2H, J = 8.3 Hz), 7.10 (m, 11H), 7.00 (m, 6H), 4.21 (t, 2H, J = 6.9 Hz), 1.73 (m, 2H), 0.58 (m, 2H), 0.07 (s, 6H). ^{13}C NMR (100.61 MHz, $CDCl_3$): δ 166.7, 148.8, 143.4, 143.2, 142.5, 140.2, 131.4, 131.3, 129.1, 128.4, 128.0, 127.9, 127.0, 126.9, 126.8, 67.5, 22.9, 14.4, 0.4. ^{29}Si NMR (79.49 MHz, $CDCl_3$): δ 22.0, -100.3. IR (thin film): ν = 3421, 3075, 3055, 3022, 2924, 2852, 1717, 1606, 1492, 1444, 1405, 1384, 1273, 1177, 1102, 1051, 841, 761, 749, 699, 627 cm^{-1}. MALDI-TOF: [M] calcd for $C_{256}H_{248}O_{36}Si_{16}$, m/z 4350.05; found, m/z 4350.60. Anal. Calcd for $C_{256}H_{248}O_{36}Si_{16}$: C, 70.68; H, 5.75; Si, 10.33. Found: C, 70.59; H, 5.81; Si, 10.31.

Acknowledgement

The authors would like to acknowledge the financial support (Grant No.: 1321760011) from the Institute of Materials Research and Engineering (IMRE), Agency for Science, Technology and Research (A*STAR).

Notes and References

1 (a) P. Li, Y. He, J. Guang, L. Weng, J. C. Zhao, S. Xiang, B. Chen, *J. Am. Chem. Soc.*, 2014, **136**, 547; (b) X. Hou, Z. Wang, M. Overby, A. Ugrinov, C. Oian, R. Singh, Q. R. Chu, *Chem. Commun*., 2013, 5209; (c) X. Z. Luo, X. J. Jia, J. H. Deng, J. L. Zhong, H. J. Liu, K. J. Wang, D. C. Zhong, *J. Am. Chem. Soc*., 2013, **135**, 11684; (d) A. I. Cooper, *Angew. Chem., Int. Ed*., 2012, **51**, 7892; e) Y. He, S. Xiang, B. Chen, *J. Am. Chem. Soc*., 2011, **133**, 14570.

2 (a) T. Li, J. E. Sullivan, N. L. Rosi, *J. Am. Chem. Soc*., 2013, **135**, 9984; (b) S. Pullen, H. Fei, A. Orthaber, S. M. Cohen, S. Ott, *J. Am. Chem. Soc*., 2013, **135**, 16997; (c) A. Foucault-Collet, K. A. Gogick, K. A. White, S. Villette, A. Pallier, G. Collet, C. Kieda, T. Li, S. J. Geib, N. L. Rosi, S. Petoud, Proc. *Natl. Acad. Sci. U.S.A*., 2013, **110**, 17199; (d) J. D. Rocca, D. Liu, W. Lin, *Acc. Chem. Res*., 2011, **44**, 957; e) A. Carné, C. Carbonell, I. Imaz, D. Maspoch, *Chem. Soc. Rev*., 2011, **40**, 291.

3 (a) J. D. Evans, C. J. Sumby, C. Doonan, *J. Chem. Soc. Rev*., 2014, **43**, 5933; (b) J. Park, L.-B. Sun, Y.-P. Chen, Z. Perry, H.-C. Zhou, *Angew. Chem., Int. Ed*., 2014, **53**, 5842; (c) H.-L. Jiang, D. Feng, K. Wang, Z.-Y. Gu, Z. Wei, Y.-P. Chen, H.-C. Zhou, *J. Am. Chem. Soc*., 2013, **135**, 13934; (d) Q. Tang, S. Liu, Y. Liu, J. Miao, S. Li, L. Zhang, Z. Shi, Z. Zheng, *Inorg. Chem*., 2013, **52**, 2799; (e) S. S. Nagarkar, B. Joarder, A. K. Chaudhari, S. Mukherjee, S. K. Ghosh, *Angew. Chem., Int. Ed*., 2013, **52**, 2881; (f) L. E. Kreno, K. Leong, O. K. Farha, M. Allendorf, R. P. Van Duyne, J. T. Hupp, *Chem. Rev*., 2012, **112**, 1105.

4 (a) G. Férey, M. Haouas, T. Loiseau, F. Taulelle, *Chem. Mater*., 2014, **26**, 299; (b) B. Liu, M. Tu, R. A. Fischer, *Angew. Chem., Int. Ed*., 2013, **52**, 3402; (c) Z. R. Herm, B. M. Wiers, J. A. Mason, J. M. van Baten, M. R. Hudson, P. Zajdel, C. M. Brown, N. Masciocchi, R. Krishna, J. R. Long, *Science,* 2013, **340**, 960; (d) A. M. Bohnsack, I. A. Ibarra, V. I. Bakhmutov, V. M. Lynch, S. M. Humphrey, *J. Am. Chem. Soc*., 2013, **135**, 16038; (e) O. Karagiaridi, M. B. Lalonde, W. Bury, A. A. Sarjeant, O. K. Farha, J. T. Hupp, *J. Am. Chem. Soc*., 2012, **134**, 18790.

5 (a) M. Mastalerz, I. M. Oppel, *Angew. Chem., Int. Ed*., 2012, **51**, 5252; (b) Y. B. He, S. C. Xiang, B. L. Chen, *J. Am. Chem. Soc*., 2011, **133**, 14570; (c) W. Yang, A. Greenaway, X. Lin, R. Matsuda, A. J. Blake, C. Wilson, W. Lewis, P. Hubberstey, S. Kitagawa, N. R. Champness, M. Schröder, *J. Am.*

Chem. Soc., 2010, **132**, 14457.
6 J. B. Birks, *Photophysics of Aromatic Molecules;* Wiley: London, 1970.
7 (a) H. Zhou, F. Liu, X. Wang, H. Yan, J. Song, Q. Ye, B. Z. Tang, J. Xu. *J. Mater. Chem. C,* 2015, **3**, 5490; (b) Y. Guo, X. Feng, T. Han, S. Wang, Z. Lin, Y. Dong, B. Wang, *J. Am. Chem. Soc*., 2014, **136**, 15485; (c) H. Zhou, J. Li, M. H. Chua, H. Yan, B. Z. Tang, J. Xu, *Polym. Chem*., 2014, **5**, 5628; (d) H. Zhou, Q. Ye, W. T. Neo, J. Song, H. Yan, Y. Zong, B. Z. Tang, T. S. A. Hor, J. Xu, *Chem. Commun*., 2014, **50**, 13785; (e) R. Hu, J. L. Maldonado, M. Rodriguez, C. Deng, C. K. W. Jim, J. W. Y. Lam, M. M. F. Yuen, G. Ramos-Ortiz, B. Z. Tang, *J. Mater. Chem.,* 2012, **22**, 232; (f) N. B. Shustova, A. F. Cozzolino, M. Dincă, *J. Am. Chem. Soc*., 2012, **134**, 19596; (g) F. Mahtab, Y. Yu, J. W. Y. Lam, J. Liu, B. Zhang, P. Lu, X. Zhang, B. Z. Tang, *Adv. Funct. Mater.,* 2011, **21**, 1733; (h) Y. Xu, L. Chen, Z. Guo, A. Nagai, D. Jiang, *J. Am. Chem. Soc*., 2011, **133**, 17622.
8 (a) Z. Sun, Y. Li, L. Chen, X. Jing, Z. Xie, *Cryst. Growth. Des*., 2015, **15**, 542; (b) B. B. Shustova, B. D. McCarthy, M. Dincă, *J. Am. Chem. Soc*., 2011, **133**, 20126.
9 M. F. Roll, J. W. Kampf, Y. Kim, E. Yi, R. M. Laine, *J. Am. Chem. Soc.,* 2010, **132**, 10171.
10 L. Zhang, Q. Yang, H. Yang, J. Liu, H. Xin, B. Mezari, P. C. M. M. Magusin, H. C. L. Abbenhuis, R. A. van Santen, C. Li, *J. Mater. Chem*., 2008, **18**, 450.
11 Y. Wada, K. Iyoki, A. Sugawara-Narutaki, T. Okubo, A. Shimojima, *Chem. Eur. J.,* 2013, **19**, 1700.
12 J. J. Ou, Z. B. Zhang, H. Lin, J. Dong, H. F. Zou, *Anal. Chim. Acta,* 2013, **761**, 209.
13 (a) I. Nischang, O. Bruggemann, I. Teasdale, *Angew. Chem., Int. Ed.,* 2011, **50**, 4592; (b) F. Alves, P. Scholder, I. Nischang, *Appl. Mater. Interfaces,* 2013, **5**, 2517.
14 (a) J. C. Groen, L. A. A. Peffer, J. Pérez-Ramírez, *Microporous Mesoporous Mater*., 2003, **60**, 1. (b) F. Rodríguez-Reinoso, M. Molina-Sabio, *Adv. Colloid Interface Sci.,* 1998, **76-77**, 271.
15 S. Liu, Z. Xiang, Z. Hu, X. Zheng, D. Cao, *J. Mater. Chem.,* 2011, **21**, 6649.
16 (a) K. Jayaramulu, R. P. Narayanan, S. J. George, T. K. Maji, *Inorg. Chem*., 2012, **51**, 10089; (b) B. Chen, L. Wang, Y. Xiao, F. R. Fronczek, M. Xue, Y. Cui, G. Qian, *Angew. Chem., Int. Ed*., 2009, **48**, 500.
17 (a) X. Wang, C. M. Cho, W. Y. Say, A. Y. X. Tan, C. He, H. S. O. Chan, J. Xu, *J. Mater. Chem*., 2011, **21**, 5248; (b) C. X. Zhang, T. J. Bunning, R. M. Laine, *Chem. Mater*., 2001, **13**, 3653; (c) G. H. Mehl, A. J. Thornton, J. W. Goodby, *Mol. Cryst. Liq. Cryst.,* 1999, **332**, 455; (d) F.-H. Kreuzer, R. Maurer, P. Spes, *Makromol. Chem. Macromol. Symp*., 1991, **50**, 215.
18 W. Cho, H. J. Lee, G. Choi, S. Choi, M. Oh, *J. Am. Chem. Soc*., 2014, **136**, 12201.

Graphic Abstract

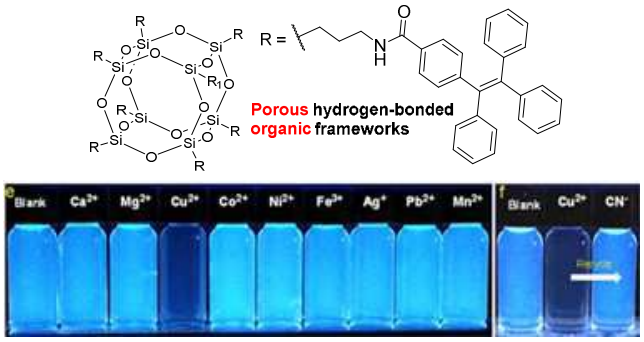

A hydrogen-bonded organic framework derived from a polyhedral oligomeric silsesquioxane and an aggregation-induced emission luminogen tetraphenylethene derivative was reported.